Supporting Information for

The Effect of Surfactants on Hydrate Particle Agglomeration in Liquid Hydrocarbon Continuous Systems: A Molecular Dynamics Simulation Study

Bin Fang[1], Fulong Ning[12]*, Sijia Hu[3], Dongdong Guo [1], Wenjia Ou[1], Cunfang Wang[4], Jiang Wen[4], Jiaxin Sun[1], Zhichao Liu[1], Carolyn A. Koh[3*]

1 National Center for International Research on Deep Earth Drilling and Resource Development, Faculty of Engineering, China University of Geosciences, Wuhan, Hubei 430074, China.

2 Laboratory for Marine Mineral Resources, Qingdao National Laboratory for Marine Science and Technology, Qingdao 266237, China

3 Center for Hydrate Research, Chemical and Biological Engineering Department, Colorado School of Mines, Golden, Colorado 80401, United States

4 CNPC offshore engineering company limited, Beijing, 100028, China

Methodology

1 Surface adsorption model

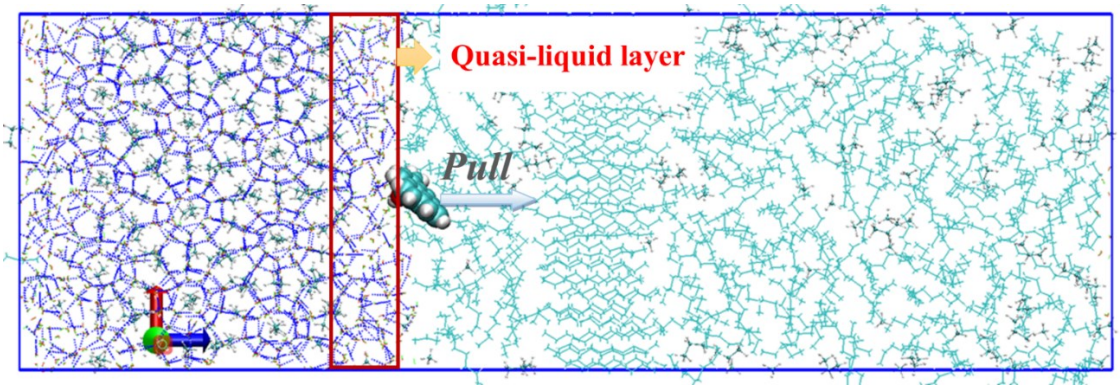

Fig. S1 Initial hydrate/hydrocarbon structure with the surfactants binding to the surface of hydrate. Red box represent the quasi-liquid layer in simulation.

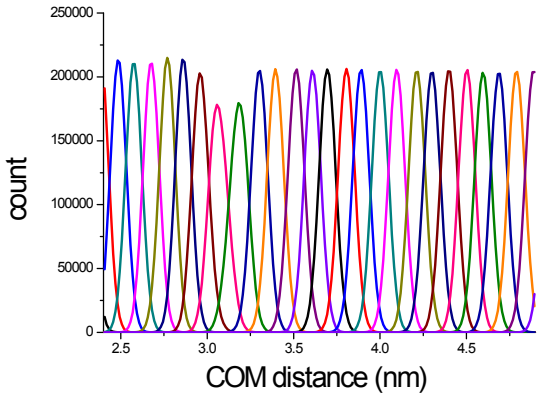

(a)

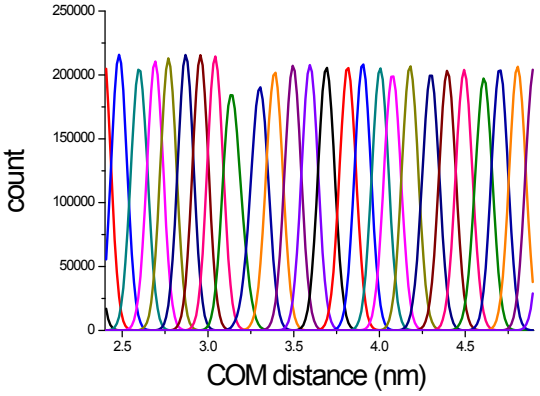

(b)

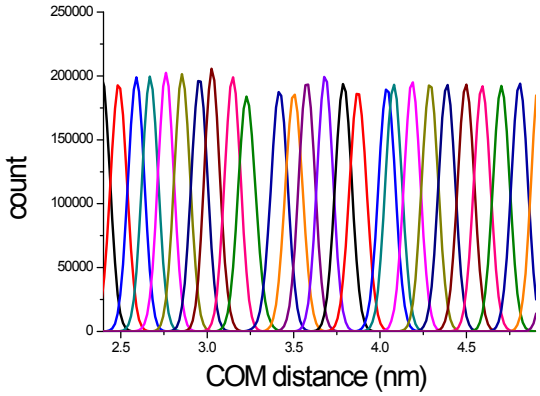

(c)

Fig. S2 Umbrella histograms for the three MD simulations with (a)1-phenylacetic acid, (b) 2-napthylacetic acid, and (c)1-pyreneacetic acid, respectively.

The simulation results show that there is a quasi-liquid layer at the hydrate surface. In order to determine which water molecules belong to the quasi-liquid phase or hydrate phase, the F_3 order parameter developed

by Baez and Clancy[1] was used to characterize the local states of the water molecules.

$$F_{3,i} = \left\langle \left[\cos\theta_{jik} \left| \cos\theta_{jik} \right| + \cos^2 104.25 \right]^2 \right\rangle_{j,k} = \begin{cases} \sim 0.1 & \text{liquid water} \\ \sim 0.0 & \text{solid water (ice,hydrate)} \end{cases} \quad \text{(S1)}$$

where θ_{jik} is the angle constituted by three adjacent water oxygen atoms (i,j,k), and the ith water oxygen atom locates at the center. Fig. S3 presents the F_3 order parameter of each water molecule (red circle) and the average F_3 values over the 1 Å interval in Z direction (blue triangle). The system with 1-phenylacetic acid is taken as an example. We conclude that the water molecules belong to the quasi-liquid phase if the average F_3 value is larger than 0.05 along the Z direction.

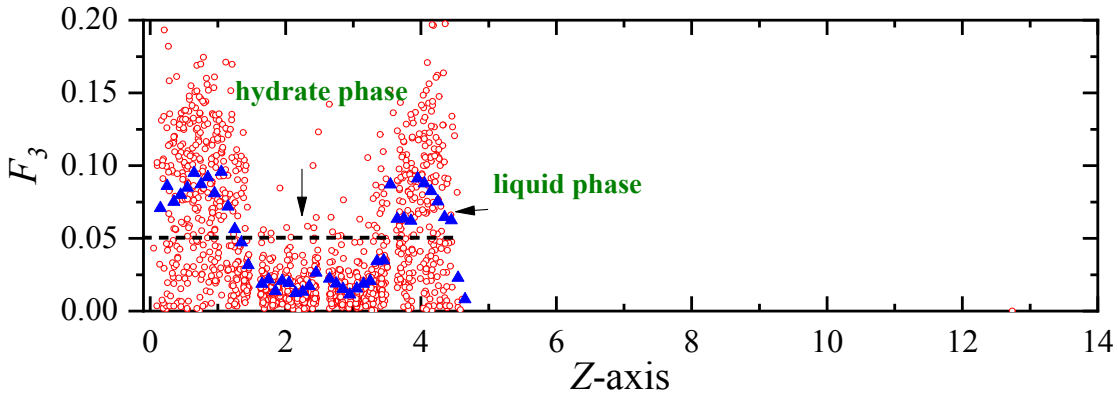

Fig. S3 The F_3 order parameter of each water (red circle) and the average F_3 value in Z direction (blue triangle).

Then, we calculated the rotational correlation function and the intermediate scattering function to ensure that the equilibration simulation time is long enough. The rotational correlation function is as follows. [2]

$$C_\alpha(t) = \left\langle P_n \left[\boldsymbol{u}(0) \cdot \boldsymbol{u}(t) \right] \right\rangle \quad \text{(S2)}$$

Where P_n is the nth-rank Legendre polynomial, we used a first order Legendre polynomial here; $\boldsymbol{u}$ is a vector attached to the molecule, we defined that the vector was perpendicular to the HOH water plane here. The rotational correlation function of water molecules in liquid phase with simulation time increase is shown in the following Figure.

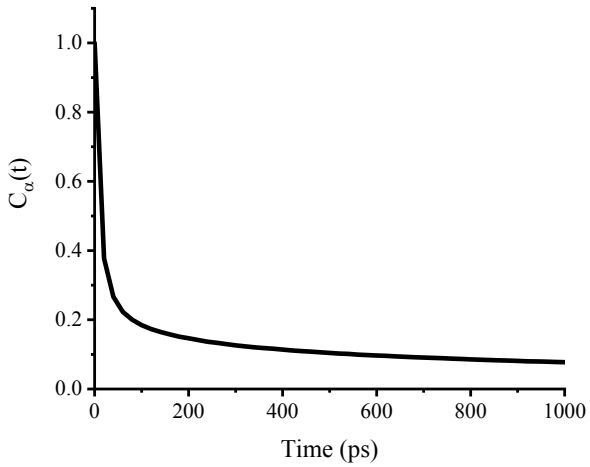

Fig. S4 The rotational correlation function of water molecules in quasi-liquid phase

The intermediate scattering function are showed in eqn S3 and S4.[3]

$$F^T(Q,t) = \left\langle \exp\left\{ i\boldsymbol{Q}\cdot\left(\boldsymbol{r}^{CM}(t) - \boldsymbol{r}^{CM}(0)\right)\right\}\right\rangle \tag{S3}$$

$$F^R(Q,t) = \left\langle \exp\left\{ i\boldsymbol{Q}\cdot\left(\boldsymbol{d}(t) - \boldsymbol{d}(0)\right)\right\}\right\rangle \tag{S4}$$

whereas $\boldsymbol{r}^{CM}(t)$, $\boldsymbol{r}^{CM}(0)$ is a radius vector of oxygen atom of water molecules at time t and time 0 respectively; $\boldsymbol{d}$ is radius vector of a hydrogen atom with respect to oxygen atom of water molecule.$\boldsymbol{Q}$ is wave vector transfer; $F^T(Q,t)$ and $F^R(Q,t)$ are translational and rotational intermediate scattering functions respectively, which can easily be calculated from MD simulation trajectories. Here, we gave the variation of translational and rotational intermediate scattering functions calculated from MD simulation trajectories with time t at Q=1.26Å^{-1}, the typical Q value is references to the Milischuk's work.[4]

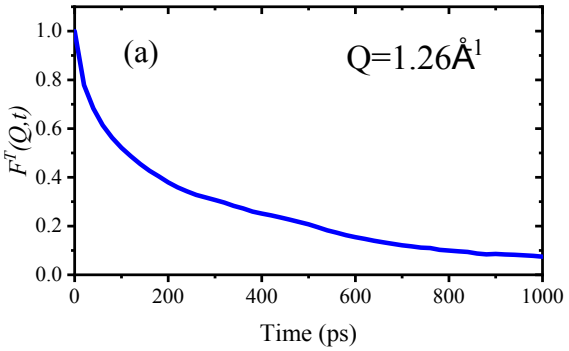

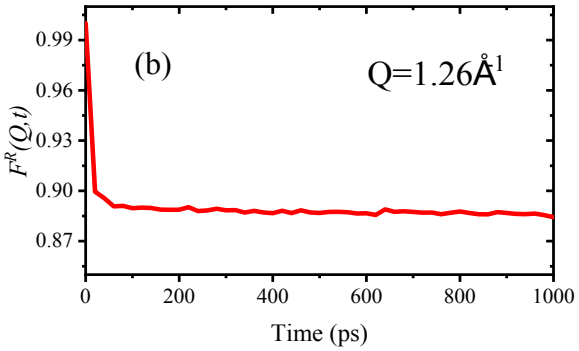

Fig. S5 Translational (a) and rotational (b) intermediate scattering functions of quasi-liquid phase water molecules

According to the rotational correlation function and the intermediate scattering function calculation, the quasi-liquid phase at the hydrate surface is well equilibrated within 1ns, which confirms that the equilibration simulation time is much longer than the orientational and translational relaxation time.

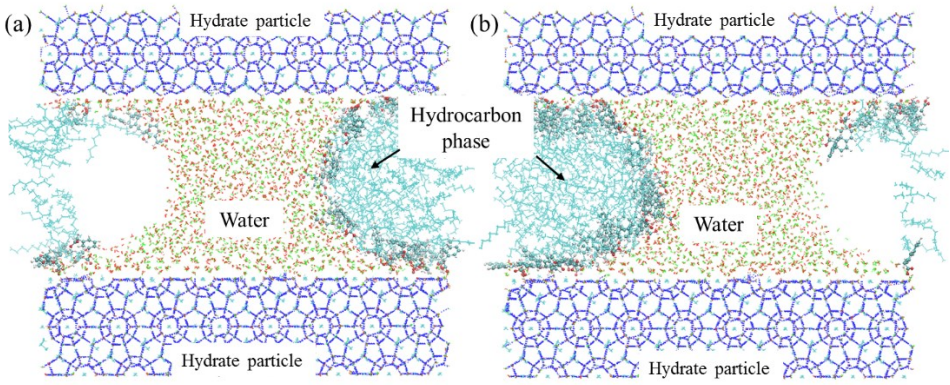

Fig.S6 Final snapshots of capillary liquid bridge model at molecular level for 1-phenylacetic acid (a) and 2-napthylacetic acid (b) systems

We further investigate the relationship between hydrate-water surface tension and bridge intensity. Here, we calculated the contact angle α between the bridge water and hydrate phase, which is closely related to the surface tension. The contact angle calulation method is similar to the Bagherzadeh's work.[5] The difference is that a ~5 Å arc of the meniscus near the hydrate surface is selected to draw a straight tangent line in all cases, shown in Fig. S7, which yield R^2 value larger than 0.92. The average of the tangents at the four points of the meniscus contacting with the hydrate surface is used, and the contact angles of the three systems with different surfactants are listed in the Table S1.

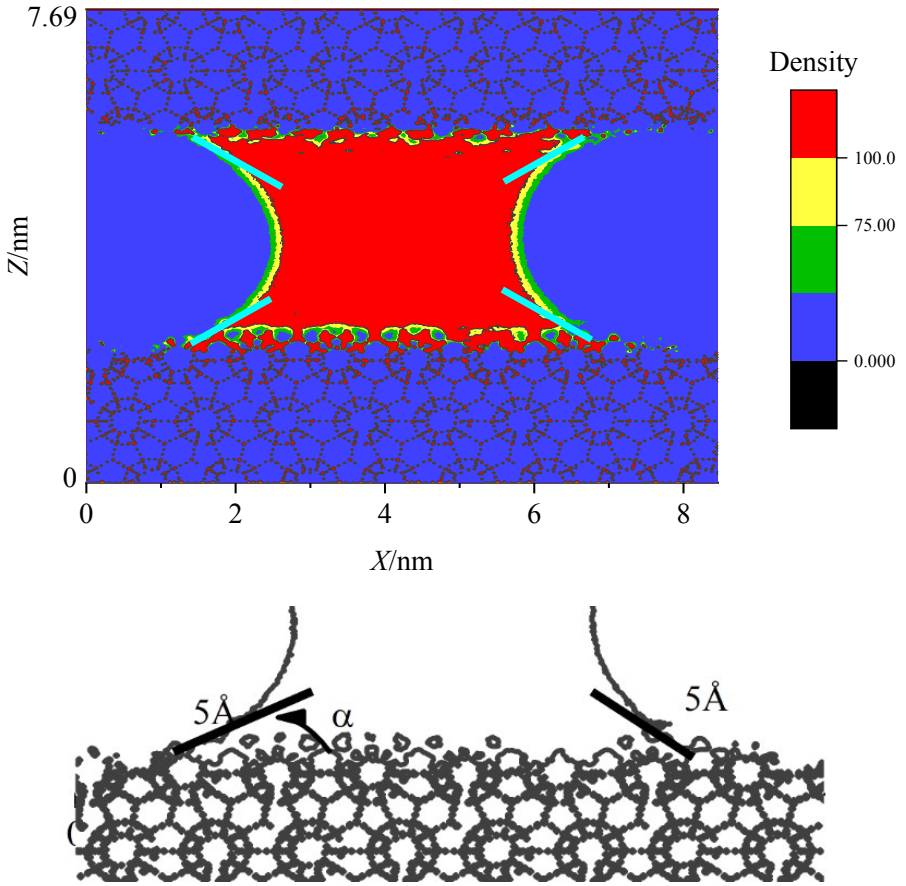

Fig. S7 Density distribution of water molecules (both in liquid bridge and hydrate phase) in the xz plane of the MD simulation. A schematic of the method for drawing tangent lines on the meniscus to determine the contact angle is shown in the bottom panel

Table S1 The calculated contact angles of the water bridge models with the three surfactants.

Systems with surfactant	Contact angle
1-Phenylacetic Acid	37.6976° ±2.7349°
2-Napthylacetic Acid	34.1098° ±1.9782°
1-Pyreneacetic Acid	40.07725° ±2.6529°

It shows that the difference of contact angle is not large and the contact angle do not show a similar trend as the H-bond number for the three systems with surfactants. This phenomenon may be induced by the limited surfactant molecules in each simulation system (only 60 surfactant molecules). Additionally, the MD simulations are limited in time and space. Therefore, the relationship between surface tension and the bridge intensity could be hardly clarified in our simulations. In the further work, we will increase the surfactant

number in simulation system and investigate the effect of surfactants on surface tension.

Pressure may be a main factor to control the decrease of H-bond number. In order to better understand the relationship between pressure and the number of H-bonds, we extended the dimension in the x direction of the 1-pyreneacetic acid simulation cells. Here, we could only extend the dimension in X direction. If we extend the dimension in Z direction, the pressure cannot change because the hydrate phase is fixed; If we extend the dimension in Y direction, the configuration of liquid bridge could be rearranged. Then, a series of simulations of the 1-pyreneacetic acids systems in different model cells Lx were performed. Considering the pressure is a physical quantity with large fluctuation at the molecular level, we counted the pressure distribution of the systems with the three surfactants and those extension systems with 1-pyreneacetic acids. It shows that the distributions of pressure conform to the statistics rule and fluctuate greatly.

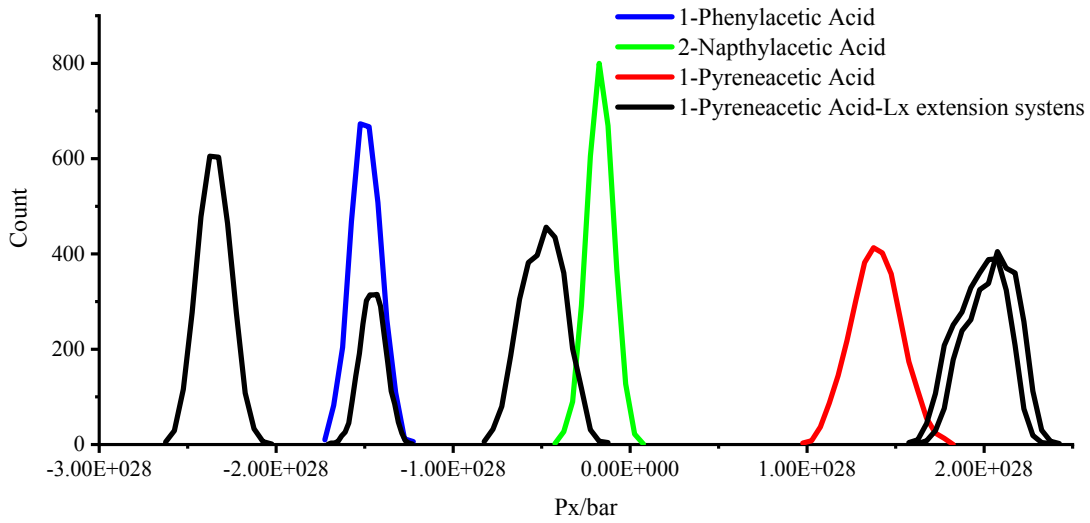

Fig. S8 The distributions of pressure in X direction.

Then we presented the average pressure Px and average H-bond number of each system in the following Fig. S9. It shows that there is no relationship between the average H-bond number and the average pressure Px of those systems with 1-pyreneacetic acids. However, no matter how the average pressure changed, the H-bond number of the 1-pyreneacetic acids systems is less than those with the other two surfactants. According to our simulations, we find the pressure has no obvious effects on H-bond number. Therefore, we think the

decrease of number of hydrogen bonds is mainly attributed to the surfactant effects.

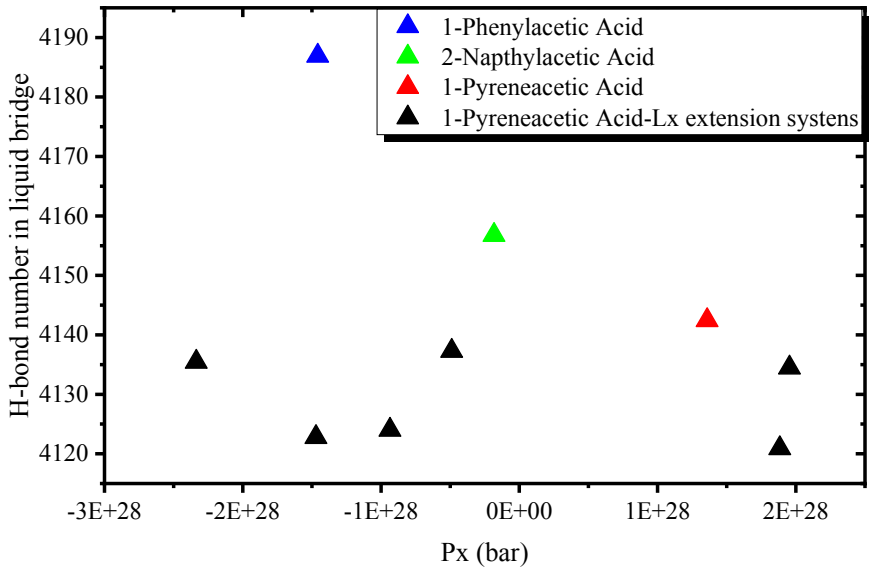

Fig. S9 The average pressure and average H-bond number of each system.

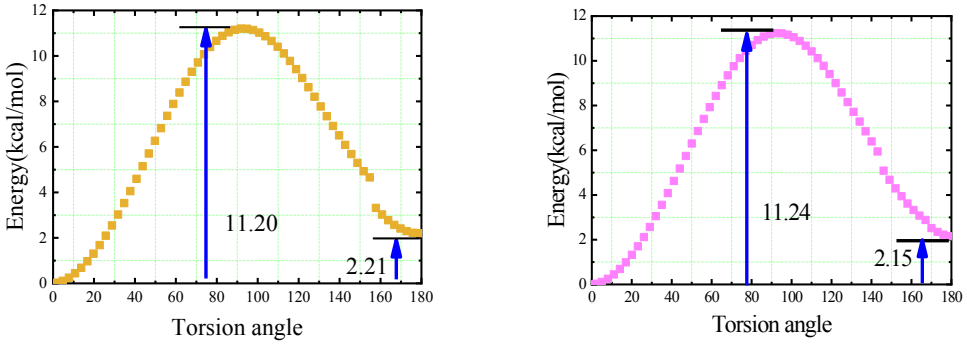

Fig. S10 Energy of 1-phenylacetic acid, 2-napthylacetic acid as an surfactant against to the carboxylic torsion angle respectively

2 AAs/water system

Three systems for the three surfactants were constructed, each consists of 8 surfactant molecules and 5700 water molecules. 10ns NPT ensemble was performed with 2ns equilibration simulation, and Van der Waals interactions were calculated using the Lennard-Jones potential with a cut-off distance of 12 Å. All simulations were performed under 10MPa and 276K condition.

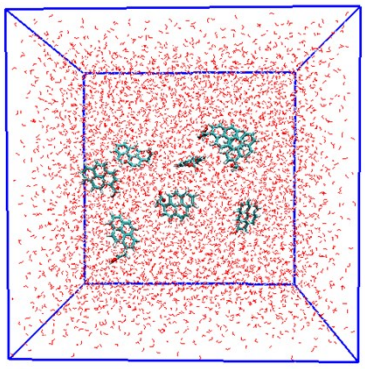

Fig. S11 Initial snapshot of surfactants/water system for MD simulation.

3. Experimental

Experimental tests were performed in order to demonstrate the kinetic inhibition of model AA.

Material

In this work, methane gas, mineral oil, naphthylacetic acid (NAA) as an AA surfactant molecule and ultrapure water are used in the experiments. Methane gas is produced by Wuhan Niuruide Trading Co., Ltd with 99.9% purity; mineral oil used in our study is provided by Dongguan Lubricating Oil Limited, and NAA is purchased from Shanghai Puhua Co., Ltd; UPW-S Millipore unit was used to produce ultrapure water, leading to the resistivity of ultrapure water more than 18.25 MΩ cm. Three types of sample fluids are prepared in this work: 1. mineral oil with 20vol.% ultrapure water (20%W/O); 2. mineral oil with 20vol.% ultrapure water and 0.5wt.% AA (20vol.%W/O+0.5wt.%NAA); 3. mineral oil with 20vol.% ultrapure water and 1wt.% AA (20vol.%W/O+1wt.%NAA)

Experimental procedure

Hydrate formation tests were performed by using the in-house HCSHW-1 experimental apparatus (Fig. S12), which has been successfully utilized in the investigation of the effect of hydrophilic silica nanoparticles added in drilling fluid on CH_4 hydrate formation in our previous work.[6] Here, the experiment was conducted at constant temperature and volume to test the kinetics of CH_4 hydrate formation with or without AA molecules. Based on the results, the effect of the AA on hydrate formation could be investigated.

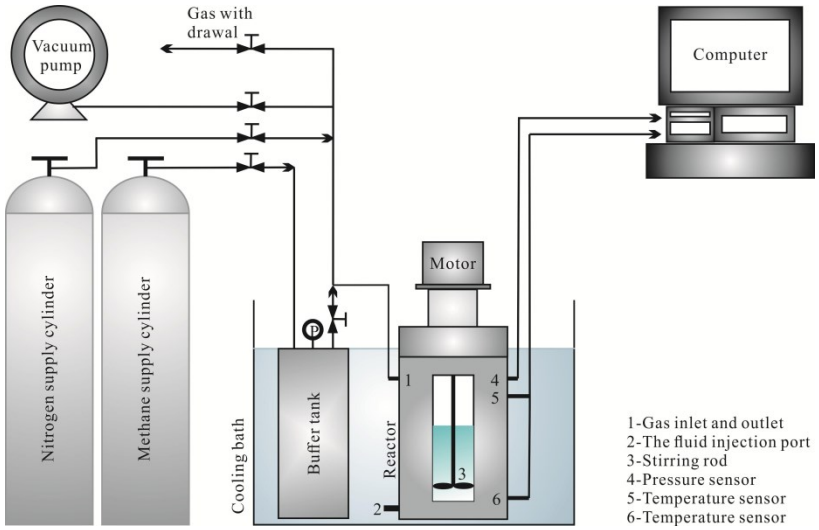

Fig. S12 Schematic of the HCSHW-1 setup.

Experimental steps are as follow:

1. Clean the apparatus and pressure test the system with N_2.

2. The 300 mL mixed sample fluid was placed into the autoclave. The remaining N_2 gas in the autoclave was extracted by a vacuum pump where the process required 10 minutes. Subsequently, the buffer vessel was pressurized by CH_4 until the pressure increased to 10.0 MPa. The temperature control system was used to cool both the liquid sample in the autoclave and CH_4 gas in the buffer vessel.

3. When the system temperature was stable at 3.0 °C. The valve of the gas inlet is opened, leading to the CH_4 gas entering the autoclave from the buffer vessel. Then the valve was closed when the pressure was increased to about 6.0 MPa. Under the above certain temperature and pressure condition, the sample fluid was stirred at the speed of the 800 r min^{-1}.

In general, the hydrate formation for the three samples was performed under the same initial temperature and pressure condition (3.0℃ and 6.0 MPa), accompanied by 800 RPM mechanical stirring. To ensure the accuracy of tests, each experimental condition was repeated for 3 times or more. The data shown in this paper were the average value.

Data processing

The variation of temperature (in both the gas and liquid phase) and pressure versus time was recorded by

the data acquisition system of HCSHW-1 experimental apparatus. Based on the variation curves, the time of nucleation (t_1) and completion (t_2) for the hydrate growth process, as well as pressure, can be determined, and the criteria was discussed in our previous work.[6]

The induction time, amount, and average rate for the hydrate formation process are of importance in evaluating the effect of AA on hydrate formation in an oil/water system. The induction time was directly quantified from the pressure variation curves; Since the gas used in the test is CH_4 with high purity, the consumption of CH_4 gas also represents the amount of hydrate formed in the autoclave, and the consumption of CH_4 gas in each test is calculated as follows:

$$\Delta n = \left(\frac{P_1}{Z_1} - \frac{P_2}{Z_2}\right) \cdot \frac{V}{RT} \tag{S5}$$

Where $\triangle n$ is the amount of CH_4 consumption, mol; R is gas constant, 8.314 J mol^{-1} K^{-1}; T is gas temperature, K; V is the gas volume, m^3; P_1 and P_2 are the initial and the final pressure for hydrate formation process, MPa, respectively; Z_1 and Z_2 are the compressibility factors under the initial and ultimately temperature-pressure conditions for hydrate formation process, respectively and calculated by natural gas deviation coefficient calculation software.

In this work, the rate of CH_4 consumption is used to characterize the formation rate of CH_4 hydrate in the experimental process, meanwhile, the calculated CH_4 gas consumption rate is described by the average consumption rate of the hydrate formation process, which can be calculated by the following equation:

$$v = \frac{\Delta n}{(t_2 - t_1)} \tag{S6}$$

Where v is the average consumption rate of CH_4, mol/min.

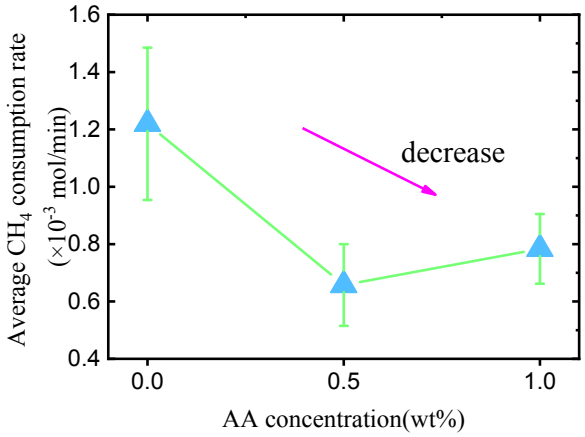

Fig. S13 The average CH_4 consumption (hydrate growth) rate for the three experiments at different AA concentrations: 20%vol.W/O; 20%vol.W/O+0.5wt.%NAA; 20%vol.W/O+ 1%wt.NAA

It is obviously shown that the average CH_4 consumption rate (namely the rate of hydrate formation) decreases when increasing the concentration of AA in oil/water samples in Fig. S13. Results indicate that the AA molecules could delay the hydrate formation process in an oil/water continuous system. In addition, the rate of hydrate formation depends on the concentrations of AAs.

1. L. A. Baez and P. Clancy, *Ann Ny Acad Sci*, 1994, **715**, 177-186.
2. D. Laage and J. T. Hynes, *J Phys Chem B*, 2008, **112**, 14230-14242.
3. S. Gautam, V. K. Sharma, S. Mitra, S. L. Chaplot and R. Mukhopadhyay, *Chemical Physics Letters*, 2011, **501**, 345-350.
4. A. A. Milischuk, V. Krewald and B. M. Ladanyi, *J Chem Phys*, 2012, **136**, 224704.
5. S. A. Bagherzadeh, P. Englezos, S. Alavi and J. A. Ripmeester, *The Journal of Physical Chemistry C*, 2012, **116**, 24907-24915.
6. R. Wang, T. L. Liu, F. L. Ning, W. J. Ou, L. Zhang, Z. Wang, L. Peng, J. X. Sun, Z. C. Liu, T. S. Li, H. C. Sun and G. S. Jiang, *J Energy Chem*, 2019, **30**, 90-100.